# Low-loaded catalyst layers for proton exchange membrane fuel cell dynamic operation part 1: Experimental study

Florent Vandenberghe, Fabrice Micoud, Pascal Schott, Arnaud Morin, Clémence Lafforgue, Marian Chatenet

▶ **To cite this version:**

Florent Vandenberghe, Fabrice Micoud, Pascal Schott, Arnaud Morin, Clémence Lafforgue, et al.. Low-loaded catalyst layers for proton exchange membrane fuel cell dynamic operation part 1: Experimental study. Electrochimica Acta, 2025, 511, pp.145364. 10.1016/j.electacta.2024.145364 . hal-04803890

**HAL Id: hal-04803890**

**https://hal.univ-grenoble-alpes.fr/hal-04803890v1**

Submitted on 26 Nov 2024

**HAL** is a multi-disciplinary open access archive for the deposit and dissemination of scientific research documents, whether they are published or not. The documents may come from teaching and research institutions in France or abroad, or from public or private research centers.

L'archive ouverte pluridisciplinaire **HAL**, est destinée au dépôt et à la diffusion de documents scientifiques de niveau recherche, publiés ou non, émanant des établissements d'enseignement et de recherche français ou étrangers, des laboratoires publics ou privés.

Distributed under a Creative Commons Attribution - NonCommercial 4.0 International License

# Low-Loaded Catalyst Layers For Proton Exchange Membrane Fuel Cell Dynamic Operation Part 1: Experimental Study

Florent Vandenberghe[1,2], Fabrice Micoud[1], Pascal Schott[1], Arnaud Morin[1], Clémence Lafforgue[1,2], and Marian Chatenet[2]

[1]*Univ. Grenoble Alpes, CEA, LITEN, 38000 Grenoble, France*
[2]*Univ. Grenoble Alpes, Univ. Savoie Mont Blanc, CNRS, Grenoble INP, LEPMI, 38000 Grenoble, France*

## Abstract

In the past decades, the proton exchange membrane fuel cell (PEMFC) components, cell/stack designs and system architecture have been significantly improved. However, despite great initial performance, PEMFC systems still suffer technological limitations, such as their initial cost, partly due to the use of expensive Pt-based electrocatalyst, which prevents widespread industrial deployment. Lowering the cathode catalyst loading while keeping high (and durable) catalytic activity has been intensively studied. In this work, low-loaded catalyst layers (20 and 100 $\mu g_{Pt}\ cm_{geo}^{-2}$) are tested in PEMFC differential single-cell (DC) under high reactant stoichiometry to characterize their intrinsic electrochemical properties under various ideal and well-controlled operating conditions of cell temperature (*T*) and relative humidity (*RH*). Particularly, the change of the membrane hydration state, via the ohmic resistance measurement, and the Pt-oxides surface coverage are investigated to gather information on the physico-chemical and electrochemical mechanisms involved in the cathode active layer, and the typical performance hysteresis observed during dynamic operation such as polarization curves. These specific electrochemical measurements further enable to build a dataset, that can be used to improve PEMFC models taking into account the complex ORR mechanism, and the role of the Pt oxides in catalyst layer transient operation and degradation.

## Keywords

Low-loaded catalyst layers; Differential cell (DC); Relative Humidity; Temperature; Membrane Hydration state; Dynamic operation; Pt-oxide surface coverage

## 1. Introduction

Proton exchange membrane fuel cells (PEMFCs) have now reached performance compatible with their commercial deployment, but still need to be improved to make them commercially successful; their cost must also be decreased, without compromising their performance and durability. Both anode and cathode catalyst layers (CLs) contain Pt nanoparticles, a significant source of material cost for PEMFCs. The kinetics of the Oxygen Reduction Reaction (ORR) being much slower than the Hydrogen Oxidation Reaction (HOR), higher Pt loadings are needed for the cathode catalyst layer (between usually 0.1 - 0.5 $mg_{Pt}$ $cm_{geo}^{-2}$) than for the anode catalyst layer (below 0.1 $mg_{Pt}$ $cm_{geo}^{-2}$) for real PEMFC applications. In that extent, more and more works aim to understand how low Pt loading cathode catalyst layer operate and perform, in order to make the link between the catalyst layer local properties, its structure and the performance [1], [2]. State-of-the-art PEMFC cathode catalyst layers have a porous nano- and micro-structure, made of Pt nanoparticles (2 to 5 nm) dispersed onto a carbon support (particle diameters between 10 to 40 nm) that are (partially) covered by a protonic conductive polymer [3], called ionomer (usually of the same chemical nature as the Proton Exchange Membrane (PEM), but made of shorter macromolecules [4]) [5]. The porous structure allows the reactive gases transport, the electronic conduction is ensured by the carbon connection network and the proton migration is possible via the hydrated ionomer film (and/or a thin film of liquid water). Electrochemical reactions take place on Pt catalytic sites that must be connected on carbon support for electronic connection and surrounded by hydrated ionomer for proton accessibility. These characteristics are mandatory for catalyst layers to operate well and to reach the highest efficiency of the PEMFC [6]. It is in fact the complex interplay of the different physico-chemical and electrochemical phenomena occurring concomitantly in operating catalyst layers that makes them the most limiting component of PEMFC.

Despite possible satisfying initial performances, lowering the Pt loading in the cathode catalyst layer remains a challenge regarding durability aspects. The lower the cathode loading, the higher the degradation rate of the performance which results in a shorter lifetime of the technology [7]. Thus, MEA manufacturers often prefer to use high cathode Pt loadings (beyond 0.25 $mg_{Pt}$ $cm_{geo}^{-2}$ loading, the ultimate target for heavy-duty transportation, given by DoE for instance) to ensure both the performance and the durability of the fuel cell.

PEMFC performance losses can be classified into two main categories: the irreversible degradations and the reversible ones. The irreversible degradations are usually connected to a non-negligible physical and/or chemical alteration of the PEMFC materials (membrane electrode assembly, MEA, and bipolar plates, BPs) and lead to non-recoverable performance losses [8], [9]. On the contrary, the reversible degradations are usually not connected to deep materials changes and deal with phenomena that contribute to a performance loss that may be recoverable under specific operation of the PEMFC [10]. Therefore, reversible losses can lead to hysteresis phenomena under dynamic operation, as observed experimentally during PEMFC performance measurements of polarization curves: the increase (forward) and decrease (backward)

current density sweeps or steps do often not superpose [11]. These reversible losses may also happen during stationary operation, resulting in a performance loss over time [12], and require a specific recovery phase to be rejuvenated [13]. Globally, these phenomena are related to the evolution of kinetics parameters, mass-transport limitations and/or abnormal (transient) local operating conditions, which can appear under specific operating conditions of the PEMFC. Among the phenomena that lead to reversible degradations, the most known are related to the water management, the Pt oxidation and the presence of impurities at the catalyst surface [14], [15]. In this work, the water management, especially the evolution of hydration state of the ionomer in the membrane and in the CL during PEMFC operation, and the Pt oxidation phenomena are investigated. The ohmic resistance evolution can be used as an indicator for the membrane hydration state, assuming the invariance of the electronic resistance of the electrodes/GDL/Bipolar plates during PEMFC operation [16]. Ge et *al.* investigated the membrane hydration state evolution at various current densities (up to 3 A $cm^{-2}$) for three gas relative humidity, thanks to different experimental tools including *operando* measurements [17]. They found that the ohmic resistance evolution is not monotonous with the current density increase from 0 up to 3 A $cm^{-2}$, because of concomitant water and heat production, two competitive phenomena occurring at high current densities.

The platinum oxidation is also identified as a phenomenon inducing ORR activity decrease at the cathode, hence PEMFC performance loss. In fact, the ORR mechanism consists of a complex multi-step reaction, which involves several surface reaction intermediates [12], [18], [19], [20]. Previous studies notably mentioned the formation of PtOH, PtO [21], [22], PtOOH [23] and $PtO_2$ [24] species, depending on the operating conditions and the way the ORR proceeds: associative [25], dissociative [26] or peroxide pathways are possible [27]. There is still no general agreement on the real description of the ORR mechanisms, and the way the formation and reduction of Pt oxides species occur in fuel cell configuration remains to be correctly described, notably to improve PEMFC operation modeling. Conway et *al.* and Jerkiewicz et *al.* agreed on the fact that surface oxygenated adsorbed species ($PtOH_{ads}$ and $PtO_{ads}$) come from water interaction with metallic Pt. At potential below 0.85 V *vs* RHE [22], [28], the surface oxidation is described by **Equation 1**.

*Equation 1 :* $$Pt + H_2O \rightarrow PtOH_{ads} + H^+ + e^-$$

Further oxidation occurs in potential range $E$ = 0.85 – 1.15 V *vs* RHE, corresponding to the formation of PtO, according **Equation 2** [28], [29].

*Equation 2 :* $$PtOH_{ads} \rightarrow PtO_{ads} + H^+ + e^-$$

Advanced characterizations are required to better understand the Pt surface oxidation and structural evolution [30], [31]. For instance, Martens et *al.* used *in situ* X-ray diffraction to probe the Pt oxides formation and reduction processes thanks to structural parameters, giving information on the adsorption of

surface electro-active species and on the place-exchange phenomenon [31]. The latter allows $OH_{ads}$ and $O_{ads}$ species to move under the Pt surface through structural transformation to form a sub-lattice [32], [33]. The slow place-exchange phenomenon somewhat hinders the surface oxide formation. They also highlighted kinetic asymmetry between oxidation and reduction sweeps, which may be ascribed to the place-exchange phenomenon, resulting in significant variation of oxide coverage during potential cycling. The evolution of the peak area and the particle size at cell voltage above 1 V *vs* RHE matches well with the onset potential of the place-exchange phenomenon referenced in the literature ($E$ > 1.10 V *vs* RHE) [33].

These phenomena are quite difficult to develop and correctly capture in modeling, mainly because of the complex interplay of the different physico-chemical mechanisms involved in the fuel cell operation and the resulting high number of parameters that must be fitted. For the sake of simplicity, Nernst and Butler-Volmer approaches in one single-step reaction are often chosen to describe the HOR and ORR; however, the ORR is a much more complex mechanism, involving the participation of several intermediates species, which questions this simplistic approach; as a matter of fact, a lot of work is carried out to unveil the ORR in operation [18], [19], [34], [35], [36]. Moreover, using Nernst and Butler-Volmer equations does not consider the Pt surface state, notably the Pt-oxides coverage and its evolution in dynamic operation. Thus, a more complex mechanistic approach, involving multiple steps of reaction, is required to get further information on the surface coverage of Pt by oxygen or hydroxyl species. Taking into account such surface coverage effects would allow to better describe the adsorption/desorption of intermediate species, as a consequence of the intermediate reaction steps occurring at the electrocatalytic sites. This description is also attractive when catalyst contamination by impurities, or electrocatalyst degradation mechanisms are considered [37], [38].

In the present study, it was decided to perform electrochemical characterizations on low-loaded catalyst layers in a differential cell setup. It is firstly done for very low Pt loading (20 $\mu g_{Pt}\ cm_{geo}^{-2}$), such low loading corresponding to very thin "0D" catalyst layers (<1 µm), that are chosen here to 'ideally' get rid of mass-transport issues (proton and oxygen transport) within the thickness of the catalyst layer; such CL are close to the ones used in the RDE and GDE set-ups. The electrochemical characterizations on very low-loaded catalyst layers in differential cell at controlled operating conditions have been validated in our previous work to compare three different electrochemical setups to benchmark the intrinsic ORR activity of state-of-the-art catalysts [39]. As fuel cell operation at such low loadings is not common, some experimental precautions must be considered to characterize the MEA in DC setup in the most reliable way. The specific choices regarding the materials, the electrochemical protocols and the operating conditions are also discussed hereafter. Then, more applicative CLs loaded at 100 $\mu g_{Pt}\ cm_{geo}^{-2}$ are also characterized to include mass-transport features and to better understand the impact of the cathode CL Pt loading and thickness on its operation. The different characterizations in this work are conducted under various operating conditions in terms of cell temperature and reactant relative humidity, to investigate the impact of these different operating

conditions on: i) the electrochemical performance along the polarization curve under oxygenated atmosphere, ii) the ohmic resistance evolution during the cathode CL operation, as well as iii) the Pt-oxides surface evolution during cyclic voltammetry measurements under nitrogen atmosphere. These combined data shall give us valuable insights, so to better understand the cathode CL operation and to discriminate and quantify the phenomena responsible for reversible losses and performance hysteresis. These experimental data should also enable to better describe our model regarding the Pt-oxides formation and reduction mechanisms, resulting in the capture of the transient Pt surface state evolution but also regarding some transport properties related to the hydration state of the membrane, this modelling work being the subject of a forthcoming paper.

## 2. Experimental

The state-of-art ORR electrocatalyst used to study the low loaded catalyst layer operation is made of 47.7% wt. Pt nanoparticles supported on Vulcan XC72 carbon support (TEC10V50E) from Tanaka Kikinzoku Kogyo (TKK), denoted Pt/VC electrocatalyst. This section describes how the anodic and cathodic catalyst layers as well as the membrane electrode assembly were manufactured, considering two different platinum loadings for the cathodic CLs: 20 and 100 $\mu g_{Pt}$ $cm_{geo}^{-2}$; these CL are denoted Pt/VC_20 and Pt/VC_100, respectively. The electrochemical characterizations and the techniques used are also presented and described below. The choice of the different materials and operating conditions are explained and discussed in the supplementary material document. The device used to conduct the electrochemical measurements is a differential cell and consists of a small active area (1.8 $cm^2$), with a thin parallel rib/channel (250 µm / 250 µm width and 400 µm depth) flow-field design to reduce the heterogeneities at the rib/channel scale (better distribution of mechanical stress and also fewer transport problems at the rib/channel scale). The use of high stoichiometric ratio for gas reactants permits to reach well controlled and homogeneous operating conditions in the electrode plane between inlet and outlet at both the anode and cathode sides.

### 2.1 Ink formulation and catalyst layer manufacture

Two catalytic inks were formulated to manufacture the anodic or cathodic catalyst layers; these inks are referred to anodic ink and cathodic ink. The anodic ink is obtained by firstly mixing the Pt/VC electrocatalyst with deionized water and pure ethanol. Milling zirconia balls (3 mm diameter) are added to the mixture, which is left on a roller mixer (IKA® ROLLER 10 basic) for an entire day for appropriate blending/dispersion. Nafion™ D2020 is added and dispersed using again the roller mixer for another 24 hours. The amounts of the different components were adjusted to reach 18% of dry content. This ink is then deposited on an inert PTFE sheet substrate (250 µm thick) using a blade-coating method. The temperature

of the coating table is set at 60°C, the speed and the height of the coating blade are set at 10 mm $s^{-1}$ and 20 µm respectively. These parameters and the ink composition were chosen to obtain anodic Pt/VC_100 catalyst layers.

The cathodic ink, which is used to manufacture cathodic catalyst layers with Pt loadings of 20 and 100 $\mu g_{Pt}\ cm_{geo}^{-2}$, is obtained by mixing Pt/VC electrocatalyst with deionized water and IPA. The mixture is firstly dispersed using magnetic stirring for 5 minutes and is then put in cold water in an ultrasonic bath for 15 minutes, twice in a row. Nafion™ D2020 is added and the final mixture is dispersed using magnetic stirring an entire day. For the cathodic ink, the solvent, the dispersion method and the dry matter content (1.5 %) are chosen to approach the ink formulation used in RDE measurements [39]. Regarding the cathode catalyst layer fabrication, the blade coating method cannot be employed to reach very low loadings such as 20 $\mu g_{Pt}\ cm_{geo}^{-2}$. Thus, the fabrication is done thanks to the spray-coating method, using a Sono-tek machine. The ink is sprayed with a flow of 0.1 mL $min^{-1}$ onto a PTFE substrate, which is fixed on a plate pre-heated at 80°C, via an ultrasonic nozzle with a speed of 30 mm $s^{-1}$. Four passes are done to reach the targeted Pt-loading of 20 $\mu g_{Pt}\ cm_{geo}^{-2}$ and the coated surface is 15 cm² (3 cm x 5 cm). To reach a loading of 100 $\mu g_{Pt}\ cm_{geo}^{-2}$, the number of passes is set to 20 and the surface of the coated cathode catalyst layer is 49 cm² (7 cm x 7 cm).

Once the catalyst layers are manufactured, the structural homogeneity and the loading of the latter are investigated carrying out surface Scanning Electron Microscopy (SEM) and X-Ray Fluorescence (XRF) measurements, respectively. The main advantage of XRF measurements is that the technique is non-destructive and gives an overview of the loading homogeneity of the catalyst layers (which is important as the large manufactured layers are cut into smaller pieces for reproducibility measurements of DC operation). The XRF characterisations are carried out using a FISCHERSCOPE® X-RAY XDV®-SDD equipment. For the very low-loaded catalyst layer, 24 points are exposed to X-ray with a 3 mm collimator and for 30 seconds for each point. In the case of catalyst layers with a loading of 100 $\mu g_{Pt}\ cm_{geo}^{-2}$, 64 points are analysed. Additionally, SEM is carried out with a FEG-SEM LEO 1530 from Zeiss. To be representative of the whole surface of the catalyst layer, four small squares are randomly chosen for the observation. The accelerating voltage is set at 5 kV and the detector is in InLens mode, to get images with a topographic contrast of the catalyst layer surface. **Figure 1 (a) and (b)** shows the results post-processing of the loading mapping of the CLs manufactured with Pt/VC via the spray coating process. For the Pt/VC_100 catalyst layers, the average loading obtained is equal to 90 ± 9 $\mu g_{Pt}\ cm_{geo}^{-2}$, with a loading in range of 60 to 120 $\mu g_{Pt}\ cm_{geo}^{-2}$ for the whole 49 cm² surface (**Figure 1 (a)**). Such analysis makes it possible to rule out any presence of areas with unsuitable loadings (affected for instance by border effects during coating) when preparing the catalyst-coated membranes (CCMs). For the Pt/VC_20 catalyst layers, the average loading obtained is equal to 20 ± 1 $\mu g_{Pt}\ cm_{geo}^{-2}$, with a loading in range of 16 to 24 $\mu g_{Pt}\ cm_{geo}^{-2}$ for the whole 15 cm² surface **(Figure 1 (b))**. The average loading is close to the target values of 100 $\mu g_{Pt}\ cm_{geo}^{-2}$ and 20 $\mu g_{Pt}\ cm_{geo}^{-2}$, with

a reasonable average dispersion over the CL geometric surface area (5% to 10%). The **Figure 1 (c)** displays a representative SEM micrograph of the Pt/VC_20 CL manufactured by spray-coating. The image shows a porous and levelled structure, which is caused by the drying method: the catalyst layer is deposited and dried layer-by-layer with the spray coating method, due to the different passes. In addition, one can see that the Pt/VC_20 sprayed on the PTFE does not cover entirely the support as some 'holes' are visible on the surface SEM image. These physico-chemical characterizations are mandatory to check the homogeneity of the composition/microstructure of the CL before CCM/MEA assembly.

## 2.2 CCM manufacture, differential cell assembly and test bench description

After checking the loading and the surface homogeneity of the manufactured catalyst layers, the next step is the CCM fabrication by hot-decal process of the CLs onto the membrane, using a hot-press machine 3R SYNTAX 100. Two membranes were chosen: the Nafion®115, which is 127 µm thick, to limit the $H_2$ permeation and a state-of-the-art Gore MX820.15, which is 15 µm thick. The hot decal-process is done at 160°C, with a mechanical stress of 1 MPa for 10 minutes. This combination of the three parameters leads to a complete transfer of the catalyst layers from the substrate onto the membrane, whatever the Pt loading (20 $\mu g_{Pt}\ cm_{geo}^{-2}$ or 100 $\mu g_{Pt}\ cm_{geo}^{-2}$). Cross-section SEM images are performed to control the quality of the CL | Membrane interface and to measure the CL thickness as shown on the **Figure 1 (d)**. The CL | MB interface is not completely smooth and the thickness of the Pt/VC_20 CL can vary from 1.5 µm to less than 0.8 µm.

To assemble the cell, a PTFE layer used as hard stop gasket and a PET film (150 µm and 25 µm thick respectively) are combined to control the cell compression and tightness, and the active area. The opening in the PTFE hard stop gasket defines a surface area of 2 cm² to host the GDL (SIGRACET 22BB from SGL) and the opening in the PET layer put on top of it defines a surface area of 1.8 cm² (corresponding to the active surface of the electrodes). Finally, the CCM is placed and the rest of the components are assembled symmetrically.

The differential cell is mounted on a commercial FuelCon evaluator-C 70350 test bench, which can supply the reactant gases and nitrogen. The gas pressures, humidity and flow rates are imposed and controlled by the bench hard- and soft-ware. To avoid any water condensation before the cell inlets, the different connections and pipes are overheated between 10 and 30°C above the temperature of the cell, which is regulated via a DI water circuit inside the monopolar plates and a thermostatically controlled bath. The electrochemical measurements are done using a Biologic® VMP2 potentiostat equipped with a 10 A/20 V booster VMP3B-10, with the anode standing for both the reference and the counter electrodes and the cathode standing for the working electrode.

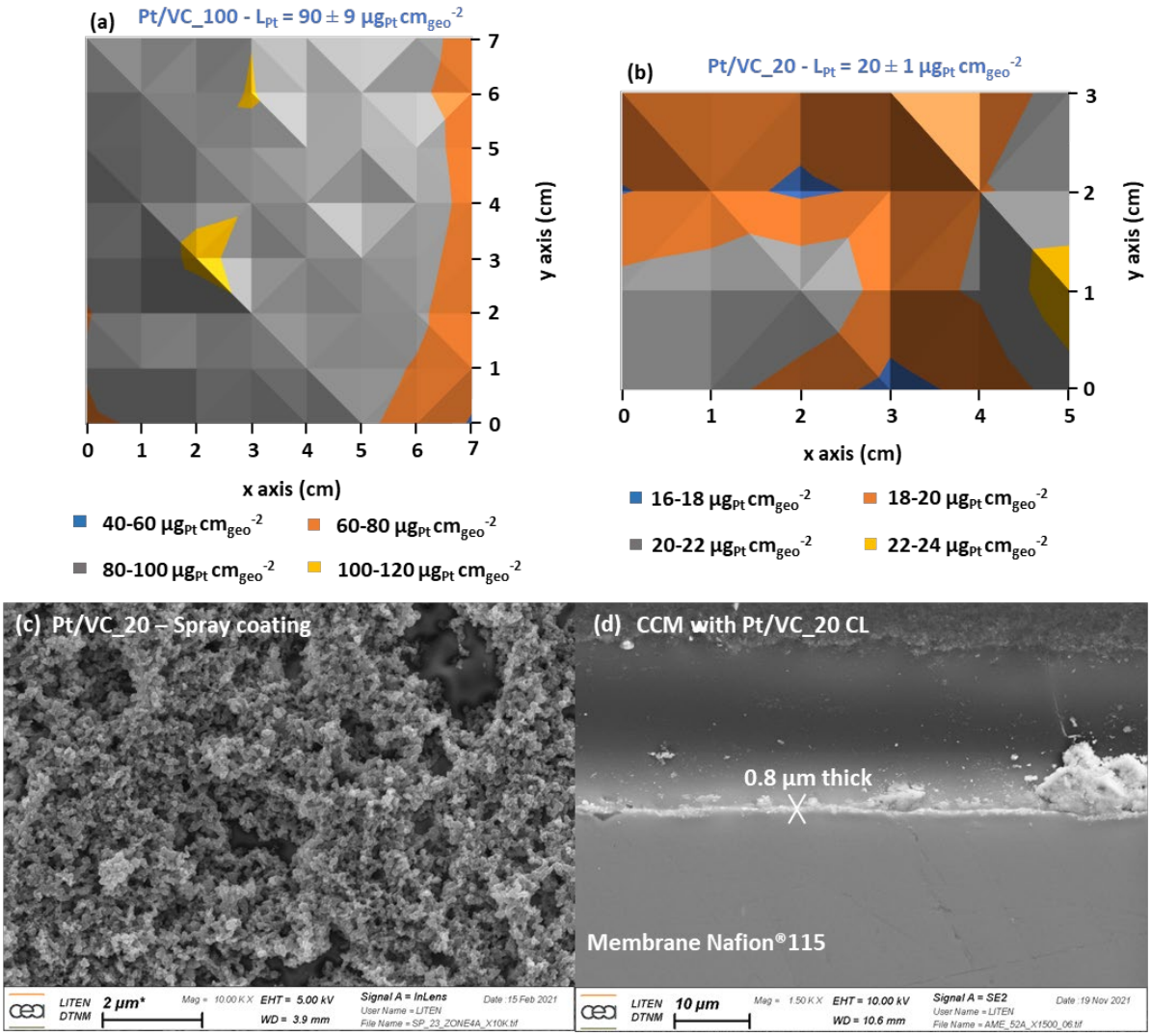


*Figure 1: Example of XRF cartographies used to control the loading homogeneity of the catalyst layers (a) Pt/VC_100 (b) Pt/VC_20. (c) Representative surface SEM image of the Pt/VC_20 CL manufactured via the spray coating method (d) Cross-section SEM image of the CCM made of Pt/VC_20 CL at the cathode.*

## 2.3 Electrochemical techniques and MEA characterizations

The electrochemical measurements are performed using the differential cell under various operating conditions of temperature and relative humidity. These operating conditions are summarized in the **Table 1**. One should know that 100% RH is obtained by setting a higher temperature of the bubbler than the cell to have liquid water in the gases. The total pressure is adjusted according to the operating conditions to keep the $O_2$ partial pressure constant. The choice of pure oxygen *vs* air at the cathode to perform some electrochemical procedure is discussed in the section **SI-1.2** of the supplementary material document.

Prior to the performance and electrochemical characterizations, a break-in procedure is performed at 80°C, 80%RH and a total pressure of 1.34 bar abs. (at both anode and cathode sides). It consists of a

stationary cell operation at 0.1 V, under $H_2$ (627 NmL $min^{-1}$) / $O_2$ (313 NmL $min^{-1}$), for both the Pt/VC_20 and Pt/VC_100 catalyst layers. This step is mandatory as it enables to activate properly the MEA to reach the nominal performances, and ensures the good operation of the MEA.

Cyclic voltammetry under $H_2$ (627 NmL $min^{-1}$) / $N_2$ (1580 NmL $min^{-1}$) configuration is used to characterize the Pt catalyst signature at the cathode. Three cyclic voltammetry cycles (CV) are carried out at 200 mV $s^{-1}$, sweeping rate at which the CV is 'correctly' shaped in the "hydrogen" and "Pt-oxide" regions for such low loadings. The third scan is always considered and shown/processed in the results. Additionally, a CV is performed at 1 mV $s^{-1}$ to capture the current density coming from the $H_2$ crossover oxidation. Indeed, at such a low sweep rate, the transient current densities produced by Pt-oxides formation/reduction reactions and proton adsorption/desorption reactions are greatly reduced, highlighting the current density coming from the $H_2$ crossover oxidation. The Pt electrochemical surface area (ECSA) is obtained by integrating the proton desorption coulometry, considering the specific coulometry of proton for bulk Pt platinum (25°C/liquid electrolyte), which is equal to 210 µC $cm_{Pt}^{-2}$.

Polarization curves are performed under $H_2$ (627 NmL $min^{-1}$) / $O_2$ (313 NmL $min^{-1}$) from OCV to 0.1 V of cell voltage, to assess the electrochemical performances of the MEA and better understand how the cathode CL operates under various operating conditions. The performance measurement is also obtained with 'fast' and successive potentiostatic impedance steps, measured every 50 mV from OCV to 0.1 V. Sixteen PEIS are performed, on the forward sweep and another 16 PEIS on the backward sweep. The potential is set for 3 seconds to avoid the influence of capacitive current due to the step transitions and then the PEIS is done from 50 kHz to 1 kHz with 10 mV amplitude, in order to make the most accurate and relevant dynamic performance measurements and ohmic drop corrections on forward and backward sweeps; it was checked that the uptime of this technique is similar to the classical polarization curve measurement performed with a fixed sweeping rate of 10 mV $s^{-1}$. More details regarding the choice of this specific protocol to perform polarization curves are provided in the section **SI-2** from the supplementary materials document.

*Table 1: Various operating conditions under which the MEA were tested in DC setup*

| **Temperature (°C)** | **Relative Humidity (anode / cathode)** | $P_{H_2O}$ **(Pa)** | $P_{H_2}$ **(Pa) /** $P_{O_2}$ **(Pa)** | **Total pressure anode/cathode (bar abs.)** |
|---|---|---|---|---|
| 30 | 100 % / 100 % | 4219 | $9.58\ 10^4$ / $9.58\ 10^4$ | $P_{atm}$ |
| 60 | 100 % / 100 % | 19917 | $9.58\ 10^4$ / $9.58\ 10^4$ | 1.16 |
| 80 | 50 % / 50 % | 23679 | $9.58\ 10^4$ / $9.58\ 10^4$ | 1.19 |
| 80 | 80 % / 80 % | 37887 | $9.58\ 10^4$ / $9.58\ 10^4$ | 1.34 |
| 80 | 100 % / 100 % | 47359 | $9.58\ 10^4$ / $9.58\ 10^4$ | 1.43 |

## 3. Results and Discussion

### 3.1 Impact of membrane thickness on CV performed on catalyst layers Pt/VC_20

The hydrogen oxidation at the working electrode, resulting from $H_2$ crossing over the membrane, is investigated thanks to a cyclic voltammetry performed at 1 mV $s^{-1}$ (**Figure 2 (a)**). The CV are performed on a MEA made of Pt/VC_20 catalyst layers with a Gore MX 820.15 membrane, in black, which is 15 µm thick and a Nafion® 115 membrane, in green, which is 127 µm thick. On the black curve, from 0.8 to 1 V, the current density is dropping from around 1.7 mA $cm_{geo}^{-2}$ to around 1 mA $cm_{geo}^{-2}$, as less Pt sites are available, due to Pt-oxides formation, hindering the complete oxidation of the $H_2$ flow. In addition, a hysteresis is observed between the oxidation and reduction sweeps, due to the asymmetry of Pt oxides formation/reduction kinetic reactions.

On the **Figure 2 (b),** the black curve, corresponding to the use of a thin membrane, is shifted towards positive current densities and centred around 1.5 mA $cm_{geo}^{-2}$ at 0.4 V; this current/voltage corresponds to the fingerprint of the $H_2$ crossover, no faradic reaction related to the Pt catalyst layer being observed in this potential region. The impact of the $H_2$ permeation on the oxidation kinetics of hydrogen can also be observed in the Pt-oxides region: an increase of the measured current from 0.75 to 0.85 V occurs, due to the concomitant Pt oxidation, before a decrease until 1.2 V. The same current density drop of 0.7 mA $cm_{geo}^{-2}$ is observed on the CV, in black, shown on **Figure 2 (b)**, which confirms that it is related to Pt-oxidation; this is a fingerprint of the $H_2$ crossover phenomenon, the corresponding HOR disturbing the description of the classical Pt-oxides region: the competition between hydrogen oxidation and Pt oxidation hinders the whole $H_2$ flow oxidation above 1 V, particularly in the case of a thin membrane with such very low Pt content. It leads to a total oxidation current density (Pt oxides formation + $H_2$ oxidation) close to the case of the use of a thick membrane (in which lower faradaic current from $H_2$ crossover oxidation is measured compared to the current from Pt oxidation). In fact, the use of a thick membrane greatly mitigates the $H_2$ crossover effect (green curve on **Figure 2 (a)**): the CV is far less shifted towards positive current (0.04 mA $cm_{geo}^{-2}$ of $H_2$ permeation) than for the black curve related to the thick membrane (1.49 mA $cm_{geo}^{-2}$). In addition, the impact of $H_2$ crossover in the Pt-oxides region is not observed for the thick Nafion® 115 membrane, leading to a "rather constant" oxidation plateau between 0.85 and 1.2 V, which results from a greatly-reduced $H_2$ crossover oxidation current.

Due to the previous observations, the thick membrane was chosen for the characterization of the Pt/VC_20 catalyst layers, instead of a thin membrane currently used in state-of-art CCMs/MEAs; this choice limits as much as possible the hydrogen crossover and its effects, which would perturbate electrochemical characterizations with such low-loaded cathode catalyst layers. The hydrogen flux that reaches the cathode, thus the permeation current produced, increases with the difference of hydrogen gas partial pressures and the permeability of the membrane, which depends on its temperature, humidification and thickness (it

increases with hydration and decreases with the membrane thickness [40]). The capacitive current generated in the different areas of the cyclic voltammetry (around 0.35 mA $cm_{geo}^{-2}$) is so low that the faradic $H_2$-crossover current has a significant impact on the measurement. Fast CV must be therefore preferred to assess correctly proton adsorption/desorption signatures, in this case at a sweeping rate of 200 mV $s^{-1}$, for Pt/VC_20 catalyst layers characterizations.

A correction from $H_2$-crossover oxidation current may be done to get rid of its signature. The correction consists of subtracting the CV performed at 1 mV $s^{-1}$ to the one performed at 200 mV $s^{-1}$. The CV corrected are shown on **Figure 2 (c)**; such correction from the $H_2$ crossover current leads to a better definition of the Pt oxides region, by "erasing" the current density drop observed at 0.8 V on the raw CV with the use of a thin membrane. In addition, the CV are centred around the x-axis at 0.4 V: the contribution of capacitive current in that potential region largely dominates and enables a more relevant comparison between CV. The different coulometries in the $H_{UPD}$ region and Pt oxides region originate from the different ECSA of the various cathode catalysts: 24 $m_{Pt}^2$ $g_{Pt}^{-1}$ for the black curve versus 29 $m_{Pt}^2$ $g_{Pt}^{-1}$ for the green curve. The impact of $H_2$-crossover oxidation on polarization curve and impedance spectroscopy under oxygenated atmosphere is discussed in the section **SI-1.1** from the supplementary material document.

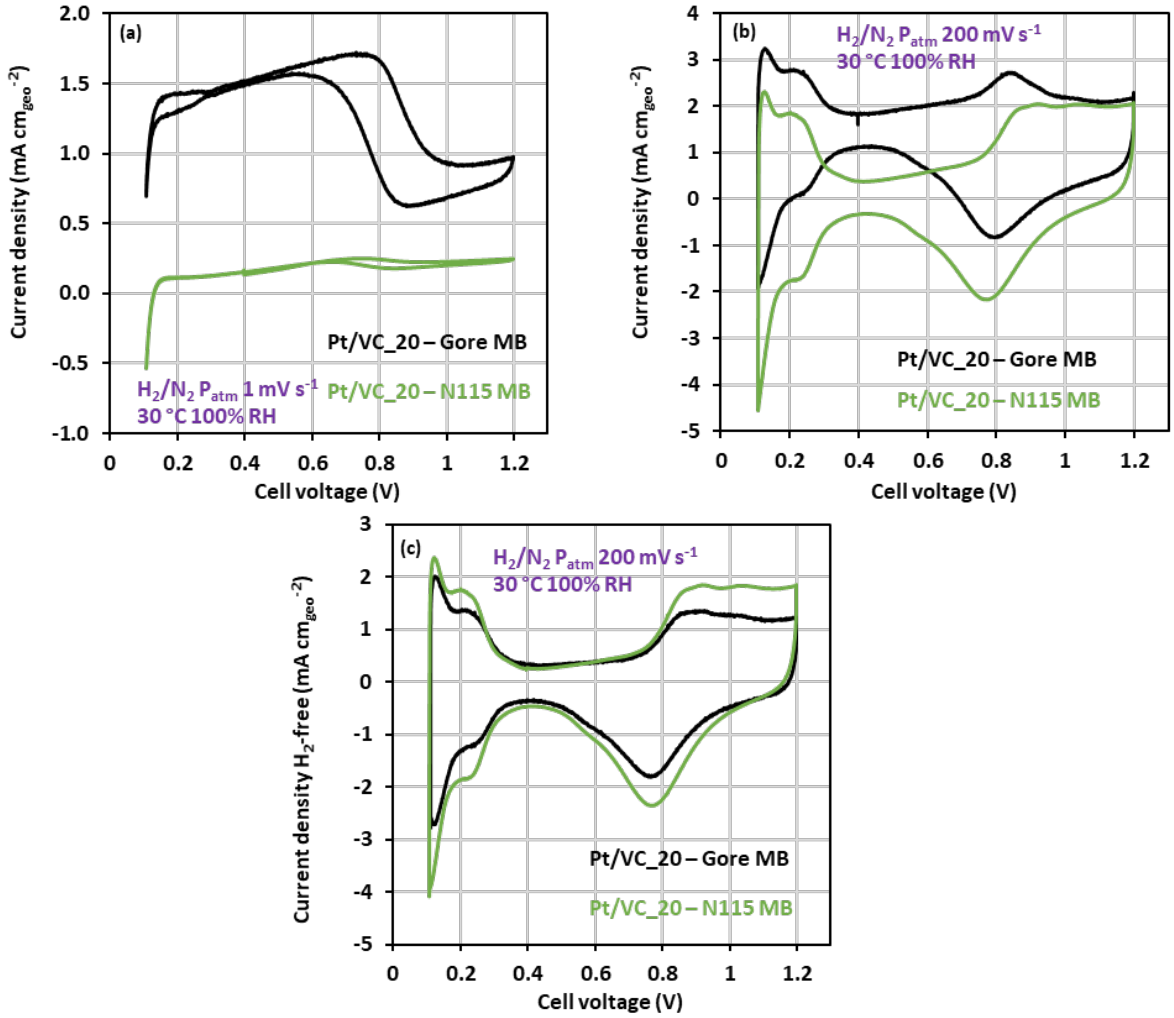


*Figure 2: (a) Voltammograms (third cycle) performed at 1 mV $s^{-1}$ on MEA made of Pt/VC_20 (b) Voltammograms (third cycle) performed at 200 mV $s^{-1}$ on MEA made of Pt/VC_20 and (c) Voltammograms performed at 200 mV $s^{-1}$ corrected from the $H_2$ permeation current at 1 mV $s^{-1}$, based on the results from Figure 2 (a) and Figure 2 (b).*

## 3.2 Qualitative evolution of Pt surface oxides coverage during CV under $H_2/N_2$ configuration

The **Figure 3 (a)** shows the third cycle of CV corrected from the $H_2$-crossover oxidation current performed at 200 mV $s^{-1}$ on MEA made of Pt/VC_20. On the latter, at 0.4 V, two currents are noticeable: a positive double layer current and a negative one. Both of them can be subtracted to the CV corrected from $H_2$-crossover current, resulting in CV corrected, from the positive and negative double layer current at 0.4 V, delimited by the two baselines represented. These corrections are done in order to get rid of the double layer capacitive current and have access to the dashed areas that solely correspond to Pt-oxides formation ($I > 0$) and reduction ($I < 0$) coulometries between 0.4 and 1 V. This range of voltage has been chosen because, according to the work of Martens et *al.*, the Pt surface state is considered only covered by surface oxides with $Pt^{+I}$ or $Pt^{+II}$ oxidation states, depending on the nature the surface oxides [31]. Indeed, a cell voltage (cathode potential) of 1 V is not high enough for the place-exchange phenomenon to occur. Moreover, below

0.4 V, the Pt surface is considered entirely reduced ($Pt^0$ state). By calculating the relative coulometries during the positive and negative scans, and thanks to a coulometry integration using the trapezoidal method, a qualitative evolution of coverage ratio of Pt surface oxides $\theta_{PtOx,s}$ (combining $PtOH_{ads}$ and $PtO_{ads}$) with potential between 0.4 and 1 V can be obtained (**Figure 3 (b)**). The presence of a hysteresis between the oxidation and reduction potential peaks can be observed. This hysteresis can be ascribed to the asymmetry of Pt oxides formation and Pt oxides reduction reactions kinetic in this range of potential or because of the slow kinetic reaction compared to the potential sweep rate. A hysteresis phenomenon can also be explained by the local hydration/dehydration of the catalyst layer, which is rather unlikely under inert atmosphere with fully hydrated gases. In other words, this hysteresis observed here implies that the Pt surface state is different for a given potential between the oxidation and reduction sweeps at the 200 mV $s^{-1}$ sweeping rate. This behaviour can partly contribute to the performance hysteresis observed during polarization curves. However, with such experimental measurements, it is difficult to have accurate insights into the type and the quantity of oxides formed, which is why modeling can be useful to extract more information about the Pt oxides formation and reduction from these experimental results.

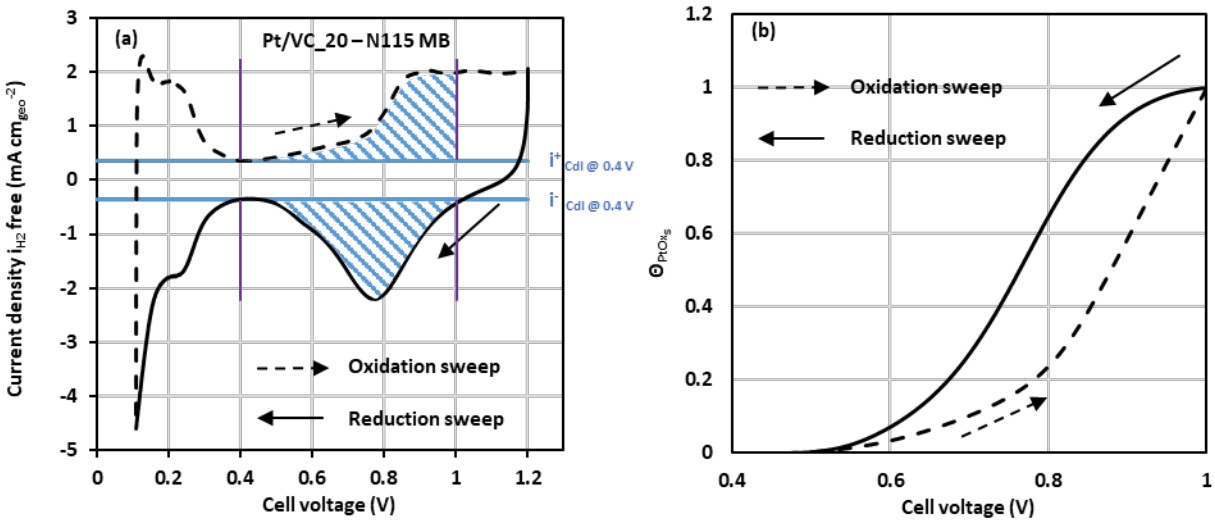


*Figure 3: (a) Voltammograms (third cycle) performed on Pt/VC_20 – N115 MB from 0.11 V to 1.2 V corrected from $H_2$-crossover current including the two capacitive baselines used to correct the CV from the positive/negative double layer current (b) Evolution of the qualitative coverage ratio of Pt surface oxides with cell voltage.*

## 3.3 Impact of operating conditions on the performance and high frequency resistance evolution under $H_2/O_2$ configuration

In this section, the impact of temperature and relative humidity on the global performance and the evolution of $R_{HF}$ with the cell voltage are investigated, for MEAs made of Pt/VC_20 and Pt/VC_100; the $O_2$ partial pressure was kept constant, by adjusting the total pressure according to the temperature and relative humidity operating conditions. The performance measurements obtained on Pt/VC_100 catalyst layers under the various operating conditions (the same as for Pt/VC_20 catalyst layers) are shown in the supplementary materials in section **SI-3**. The performance, corrected from ohmic drop, at 60°C are better than at 30°C

(**Figure 4 (a)**), which is likely due to the enhancement of ORR kinetics at higher temperature and the reduced activation losses [41], and the improved ionic conductivity and proton mobility at high temperature. Keeping constant %RH (100%), **Figure 4 (c)** shows the $R_{HF}$ evolution with potential for the three operating conditions 30, 60 and 80°C: the $R_{HF}$ values decrease as the cell temperature increases, no matter the working point considered. Note that these $R_{HF}$ values (thus, the conductivity values) are in agreement with those expected for thick Nafion® membranes [42]. At 100% RH, it is interesting to note that the $R_{HF}$ values increase with potential decrease/current density increase. This may be explained by local heat production, inducing a local drying of the membrane that counter-balances the water production. Indeed, it has been seen that the heat produced in the active layers may lead to a local overheating up to 10°C above the cell temperature set point [43]. This trend is also in agreement with the work of Ge et *al.* for one of the operating condition they investigated, corresponding to the fully hydrated inlet gas at high current density [17]. In addition, the $R_{HF}$ variations at 30°C, 100% RH are much higher than at 80°C, 100% RH: up to 40% variation compared to 20%, respectively. A possible explanation may be that, if the membrane conductivity follows an Arrhenius law, and considering that the hysteresis is driven by the pre-exponential term, which depends on the water content, the temperature evolution should affect the hysteresis amplitude. The behaviour of the polarization curve at 80°C is surprising and unexpected, with a very pronounced hysteresis between the forward and backward sweeps (at the large benefit of the backward sweep). This behaviour is actually reproducible on the present measurements; a hypothesis to account for it is that on the forward sweep, the heat production in the active layer likely overwhelms the water production (water can still be expelled "easily" from the active layer, because there is yet no "saturation" of the active layer by liquid water), resulting in depreciated proton conductivity of the ionomer. On the contrary, on the backward sweep, the performance gain may originate from non-negligible water accumulation in the ionomer, thereby decreasing the proton resistance and increasing the apparent performance of the cathode.

The impact of the relative humidity at 80°C on the global performance and on the evolution of $R_{HF}$ with the potential are shown on **Figure 4 (b)** and **(d)**, respectively. Higher hydration of the gas reactants leads to better global performance. At 100% RH, the proton conductivity is improved, which leads to better performance. This assumption is clear at 80°C on **Figure 4 (d)**: at 100% RH, the $R_{HF}$ are around 4 times lower than at 50% RH. One can notice that the evolution of $R_{HF}$ values is not monotonous: it firstly decreases with increasing current from OCP at 80°C, 50 and 80% RH, until a potential around 0.4 V from which $R_{HF}$ values start to increase. Here again, the competition between the water production and the heat production can be responsible for this effect, resulting in a progressive hydration and then a dehydration of the membrane. The work of Ge et *al.* highlighted the local heat production being responsible for this particular trend instead of the electro-osmotic drag mechanism, inducing local anode-side membrane dehydration, which is the other potential cause for membrane dehydration at high current density [17]. Another interesting point is that the forward sweep of the polarization curve obtained at 80°C, 50% RH shows better performance

for potentials varying from 0.6 to 0.4 V, than in the backward sweep. As the variation of the high frequency resistance in that specific case does not account for the phenomenon observed on the polarization curve at 80°C, 50% RH, an explanation might be the better hydration of the active layer, due to water production on the forward sweep; on the backward sweep, the benefits from the water production and better hydration seem to be significantly counterbalanced by the local heat production. However, without the variation of the protonic resistance in the catalyst layer along the polarization curve, which could not be measured due to the supposed ideal '0D' cathode catalyst layer (*i.e.* the contribution of the protonic resistance in the catalyst layer cannot be monitored by electrochemical impedance spectroscopy), it is difficult to conclude properly.

Finally, the hysteresis between the forward and backward sweeps of the polarization curves are still observed, no matter the operating conditions, even though the polarization curves are corrected by the ohmic drop at each potential step. This means that the variation of the high frequency resistance (*i.e.* the membrane resistance) is not the only phenomenon accounting for the hysteresis observed during transient operation of the PEMFC. Considering the supposed ideal '0D' catalyst layer, for which protonic conduction in the catalyst layer can be considered as non-limiting, the fact that the electrochemical signature of proton transport is not captured experimentally by the EIS measurements suggests that another phenomenon is responsible for the hysteresis. This phenomenon might be related to some sulfonic groups contamination due to ionomer adsorption/desorption on the Pt surface or to the hydration/dehydration of the CL (at the local interface with Pt), which both modify the proportion of Pt sites that can operate efficiently. This explanation is amplified with the type of carbon used, mainly porosity dependant, as it was seen in the study of Chabot et *al.* in which they observed hysteresis on the sorption isotherms performed on catalyst layer made of Pt supported on Vulcan carbon (same catalyst used in this study) and on catalyst layer made of Pt supported on high surface area carbon (more porous than the Vulcan carbon) [4]. They observed that in the case of high surface area carbon, the water uptake by the catalyst layer is larger than in the case of Vulcan carbon and the hysteresis between the sorption/desorption is bigger in the case of high surface area carbon that in the case of Vulcan carbon. From their observation, and due to the fact that the electrochemical signature of proton mobility during EIS measurement is not observed, it was decided to focus on information related to the Pt-oxides formation and reduction, which might also be responsible of the hysteresis observed between the forward and the backward sweeps of the polarization curve. This is why qualitative coverage ratio of Pt surface oxides evolution during CV under $H_2/N_2$ configuration is investigated and will be used to help developing a Pt-oxides formation/reduction mechanism in non-operating environment.

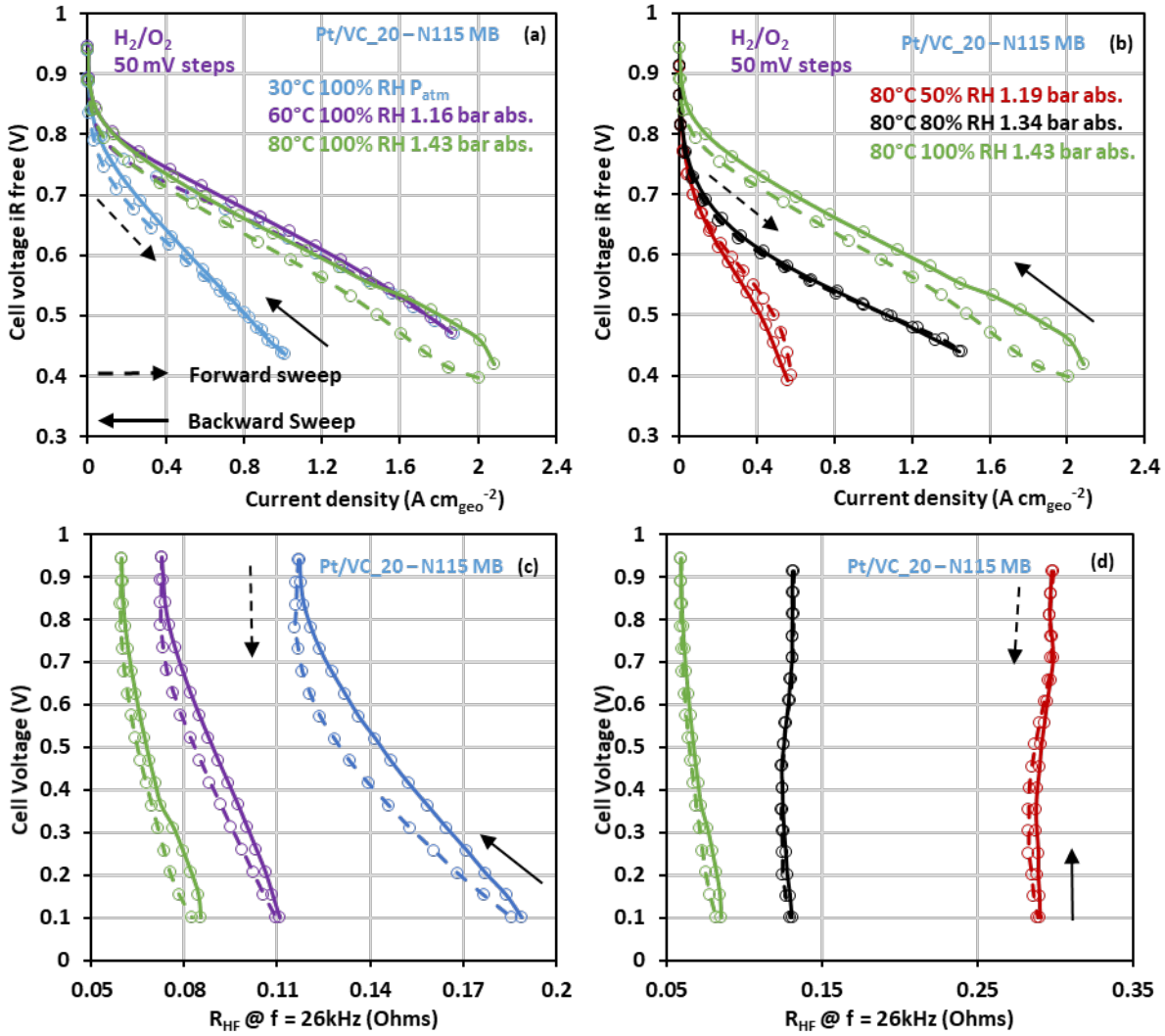


*Figure 4: Polarization curves with ohmic drop correction performed on MEA with Pt/VC_20 – N115 MB, 1.8 cm² geometric surface, at (a) different temperatures at 100% RH (b) at different relative humidities at 80°C; $R_{HF}$ evolution along the polarization curve for Pt/VC at (c) different temperatures at 100% RH and (d) different relative humidities at 80°C.*

In this section, the impact of loading on global performance and $R_{HF}$ evolution obtained at 80°C, 80% RH is investigated for catalyst layers of different thickness (loaded at 20 $\mu g_{Pt}\ cm^{-2}$ or 100 $\mu g_{Pt}\ cm^{-2}$), in which transport limitation in the catalyst layer may occur. Indeed, by opposition to '0D' catalyst layers (Pt/VC_20, 20 $\mu g_{Pt}\ cm_{geo}^{-2}$), '1D' catalyst layers (Pt/VC_100, 100 $\mu g_{Pt}\ cm_{geo}^{-2}$, 3-4 µm thick) can induce the existence of a concentration gradient within their depth, that changes the local concentration of $O_2$, and a protonic potential gradient which also modifies the local electrode potential through the thickness. Thus, the correction from Pt active surface is not fully relevant to compare polarization curves performed at these two different loadings, even though the comparison can still be done at low current density (in the region where mass-transport limitations are negligible). No matter the potential considered, the global performance of the 1D active layer is not multiplied by a factor 5, as the loading is, due to mass-transport contribution in the catalyst layer. The comparison between the two loadings has only been done at one operation condition: 80°C, 80% RH because it is the main operating condition during PEMFC operation that has been investigated

for model development. The other operating conditions can be used for further validation of the model by comparing the experimental results and the simulations.

**Figure 5 (a)** shows that larger current density is produced at 100 $\mu g_{Pt}$ $cm_{geo}^{-2}$, which leads to a bigger ohmic drop in the membrane (cell) than at 20 $\mu g_{Pt}$ $cm_{geo}^{-2}$. More water is also produced, which leads to a better hydration state of the ionomer in the active layer and in the membrane, as shown on the ($R_{HF}$ *vs* voltage) evolution (**Figure 5 (b)**). Regardless of the potential, the $R_{HF}$ values are lower in the case of Pt/VC_100 catalyst than for Pt/VC_20 catalyst layers, which might be explained by the different thicknesses of the cathode layers and the fact that the different thicknesses may induce different compression strain (the thick CL being less compressed than the thin one). This difference can also come from the CL | Membrane interface which is heterogeneous and not well defined for the CCM made of Pt/VC_20 CL contrary to Pt/VC_100 CL. Also, be it on the $R_{HF}$ evolution or polarization curves, the hysteresis between the forward and backward sweep seems to be wider in the case of Pt/VC_100 than for Pt/VC_20 catalyst layers except below 0.35 V. This may be explained by the different response through the thickness of the catalyst layer: the water retention must not be similar between the PEM and the GDL sides, leading to the wider hysteresis of $R_{HF}$ for thick catalyst layers. One should know that the electronic resistance of the Pt/VC_20 might become non-negligible and could contribute to the total high frequency resistance measured due to limited electronic contact between the carbon grains within the CL and possibly a non-homogeneous interface with the MPL. Regarding the polarization curve, the wider hysteresis may be explained by the asymmetry of the Pt-oxides formation/reduction kinetic in the case of Pt/VC_100 catalyst layers as mentioned above, Pt-oxides formation/reduction involving water (so being influenced by the hydration state of the membrane and ionomer). This probably results in different transport properties of proton, due to different hydration state of the catalyst layer between the forward sweep and backward sweep (presence of water in the porosity of the carbon support [4]). Indeed, it was seen in another study with commercial MEA that $R_{H+,CL}$ was evolving with the working point, thus, it should also evolving along the polarization curve and between the forwards and backward sweeps, as the $R_{HF}$ does [44].

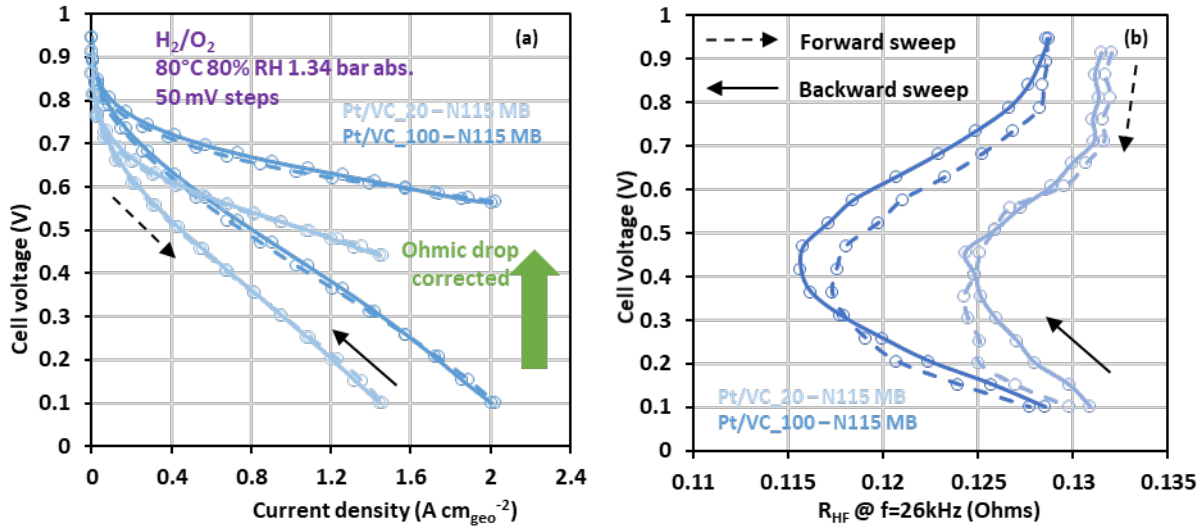


*Figure 5: (a) Second cycle of polarization curve with and without ohmic drop correction performed at different loadings for Pt/VC – N115 MB, 1.8 cm² geometric surface, and (b) corresponding $R_{HF}$ evolution along the polarization curve.*

## 3.4 Impact of operating conditions on the ECSA value and qualitative evolution of the Pt surface oxides coverage during CV under $H_2/N_2$ configuration

This section deals with the impact of the temperature and relative humidity on the ECSA of for Pt/VC_20 and Pt/VC_100 catalyst layers and on the Pt surface oxides coverage investigated by cyclic voltammetry. The voltammograms and the values of the ECSA, obtained under the different operating conditions, are calculated via the proton desorption coulometry from the CV presented on **Figure 6 (a)** and **(b)** and summarized in the **Table 2**. Firstly, at constant relative humidity, the ECSA values decrease with the temperature, a behaviour which was also observed in RDE measurements in liquid electrolyte [44]. In these calculations, it was considered that 210 µC $cm_{Pt}^{-2}$ still applies at 60 and 80°C, even though the validity of this assumption could probably be questioned (but will not be further discussed herein). Secondly, at constant temperature, the ECSA values increase with the relative humidity. This may be explained by the fact that high hydration of the catalyst layer favours proton mobility and therefore avoids/limits proton transport limitations to the Pt active sites. In addition, by reducing the relative humidity, some active sites might become non-accessible to proton, resulting in lower ECSA values. **Figure 6 (c)** shows the impact of temperature at constant relative humidity on the qualitative evolution of the Pt surface oxides coverage of the Pt/VC electrocatalyst. The hysteresis observed, related to the different positions of the potential peaks of Pt-oxides formation and reduction reactions, is wider at 30°C than at 60 and 80°C, which is consistent with the fact that at 30°C, the gap between potential peak of Pt oxidation and Pt-oxides reduction is wider than at 80°C. At 0.75 V, Pt sites are qualitatively more covered by surface oxides at 80°C than at 60 or 30°C at 100% RH, which signs that Pt-oxides formation is promoted at higher temperature. On the reduction sweep, the higher the temperature the faster the reduction, the peak related to Pt-oxides reduction being shifted towards positive potential. Overall, both Pt oxidation and Pt-oxides reduction kinetics are enhanced by temperature, resulting in a reduced gap of the peak potential of the two reactions.

The relative humidity does not seem to have a significant impact on the kinetic of Pt-oxides formation and reduction reactions, as the position of the peaks related to these reactions seem to be %RH independent (see **Figure 6 (b)**). However, the increase of the relative humidity at constant temperature seems to also promote Pt-oxides formation until 0.85 V as the integrated coulometry is bigger at higher relative humidity (**Figure 6 (d)**). Above 0.85 V, this trend is not as evident, which makes sense: water is consumed during the first Pt oxidation step (see **Equation 1**). As such, the hysteresis is wider at 50% RH than at 100% RH, with more Pt-oxides formed at 0.75 V in the case of fully hydrated gases than at 50% RH at 80°C. Above 0.85 V, further oxidation of $PtOH_{ads}$ into $PtO_{ads}$ occurs and seem to be %RH independent, which is strange as proton mobility is involved in this reaction and is %RH dependant. Regarding the reduction sweep, the RH does not seem to have a significant impact on the Pt oxides reduction kinetics, as the position of the peak is not shifted according to the relative humidity.

The trends at 80% RH and 100% RH are interesting but not simple to understand: it seems that fully hydrated gases slightly hinder the Pt-oxides formation and reduction, more Pt oxides being formed at 80% RH than at 100% RH in the potential region 0.5 - 0.7 V. However, let us stress that the value of the Pt-oxides surface coverage is probably overestimated in the region 0.5 - 0.65 V, due to carbon surface oxidation reaction/functionalization, whose signature is difficult to correct properly. Finally, the increase of temperature at constant relative humidity and the increase of relative humidity at constant temperature seem to promote the formation of quinone/hydroquinone (Q/HQ) groups [45], as the corresponding electrochemical signature (oxidation peaks observed around 0.6 V on the different CV) is more pronounced at high temperature/relative humidity, due to faster initial steps of carbon corrosion [45], [46], [47].

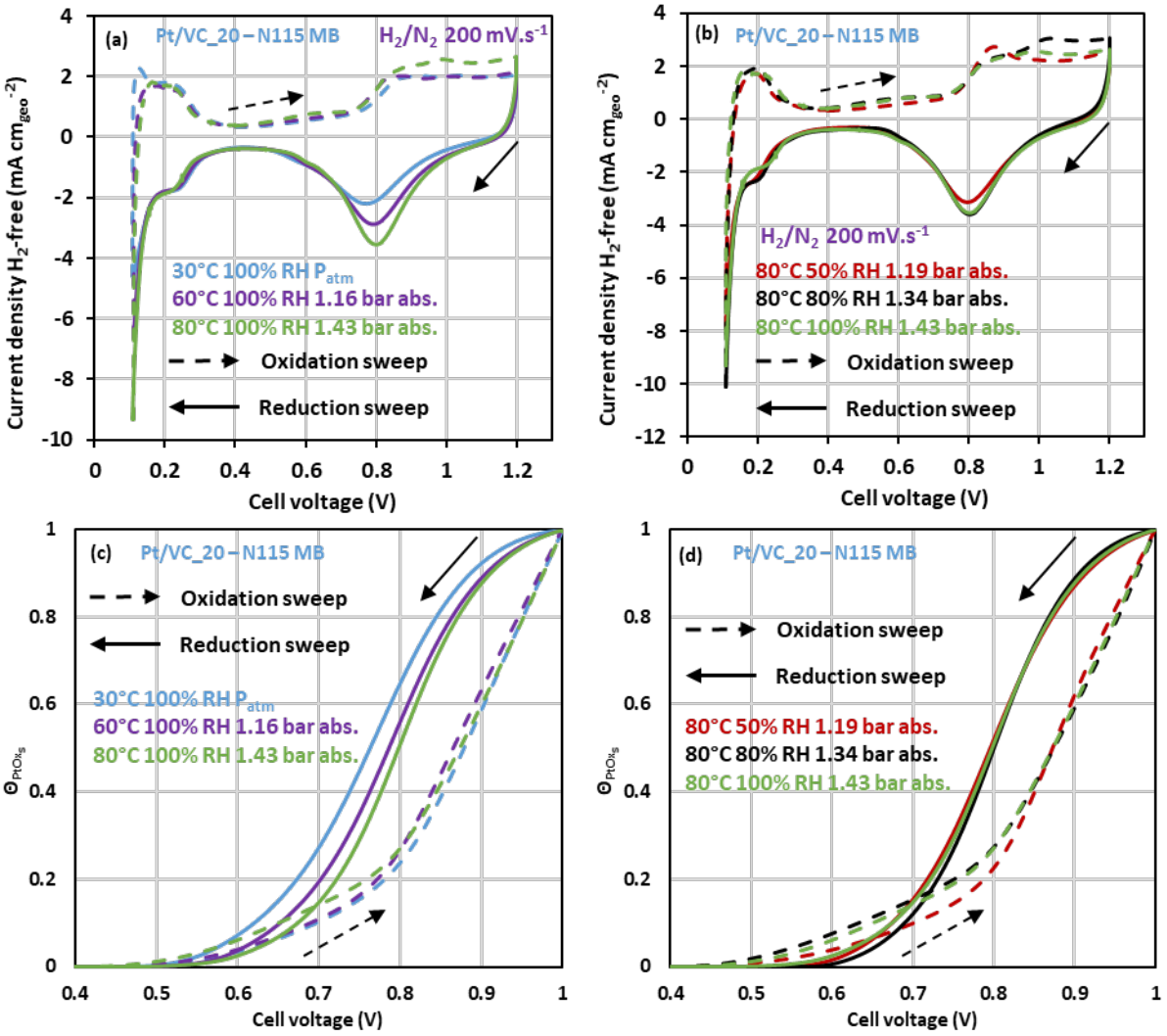


*Figure 6: Cathode voltamograms (third cycle) on MEA made of Pt/VC_20 – N115 MB, 1.8 cm² geometric surface, obtained at (a) different temperatures at constant RH and (b) different RH at constant temperature. (c) Impact of temperature on the qualitative evolution of Pt surface oxides coverage at (c) constant relative humidity and (d) at constant temperature.*

The same study as in the previous section was done considering Pt/VC_100 catalyst layers, to determine in what extent the catalyst layer thickness (3-4 µm for Pt/VC_100 catalyst layers) and loading have an impact on the different behaviours observed in the case of Pt/VC_20 catalyst layers. The characterizations are performed on MEA including the membrane Nafion® 115, as for Pt/VC_20 catalyst layers, so to change only one parameter. The different experimental results obtained on Pt/VC_100 catalyst layers under the various operating conditions are presented in **SI-4** section of the supporting information. Only one operating condition, 30 °C and 100% RH, is considered here as it will be the one considered for the model development and used when comparing experimental results with simulations from the model developed in the second part of the study.

The **Table 2** gathers the ECSA values, obtained under various characterization conditions, for Pt/VC_20 and Pt/VC_100 catalyst layers. There is almost no difference regarding the ECSA values (normalized by the loadings, expressed in $m_{Pt}^2$ $g_{Pt}^{-1}$) between the two loadings considered in this study, whatever the

experimental conditions. This means that (within the error bar) multiplying the loading by five, leads effectively to a 5 times higher surface of Pt available for proton adsorption/desorption in this loading range, sign of a rather constant Pt utilization factor [6]. Plus, the ECSA value evolution with temperature and relative humidity follows the same trend as for those obtained with catalyst layers loaded at 20 $\mu g_{Pt}\ cm_{geo}^{-2}$.

*Table 2 : ECSA value obtained under various operating conditions at both 20 and 100 $\mu g_{Pt}\ cm_{geo}^{-2}$ loadings*

| **Operating conditions** | **ECSA values ($m_{Pt}^2\ g_{Pt}^{-1}$) 20 $\mu g_{Pt}\ cm_{geo}^{-2}$** | **ECSA values ($m_{Pt}^2\ g_{Pt}^{-1}$) 100 $\mu g_{Pt}\ cm_{geo}^{-2}$** |
|---|---|---|
| 30°C / 100% RH / $P_{atm}$ | 32 ± 0.3 | 34 ± 2.1 |
| 60°C / 100% RH / 1.16 bar abs. | 28 ± 2.0 | 29 ± 2.4 |
| 80°C / 50% RH / 1.19 bar abs. | 18 ± 2.0 | 21 ± 0.2 |
| 80°C / 80% RH / 1.34 bar abs. | 21 ± 0.2 | 23 ± 2.0 |
| 80°C / 100% RH / 1.43 bar abs. | 23 ± 3.0 | 24 ± 2.2 |

The **Figure 7 (a)** shows a comparison of the CV obtained at 30°C, 100% RH normalized by the Pt active surface for proton desorption (ECSA expressed in $cm_{Pt}^2\ cm_{geo}^{-2}$) between Pt/VC_20 and Pt/VC_100 and corrected from $H_2$-crossover current. The normalization has been done to have a relevant comparison between CV obtained at different loadings. In the $H_{UPD}$ region, there are almost no differences between the two loadings. In the Pt-oxides region, there is only slight differences, that might probably come from experimental uncertainties related to the CL manufacture and the current from the double layer capacitance. This seems to be confirmed by the oxidation sweeps of the Pt surface oxides coverage ratio evolution with potential shown on **Figure 7 (b)**. On the reduction sweeps, the differences observed on **Figure 7 (b)** might be due to thickness effect, but it is also difficult to conclude reliably. Overall, the normalization by the ECSA shows that the CL behavior and Pt utilization factor seems to be the same at both 20 and 100 $\mu g_{Pt}\ cm_{geo}^{-2}$ loadings.

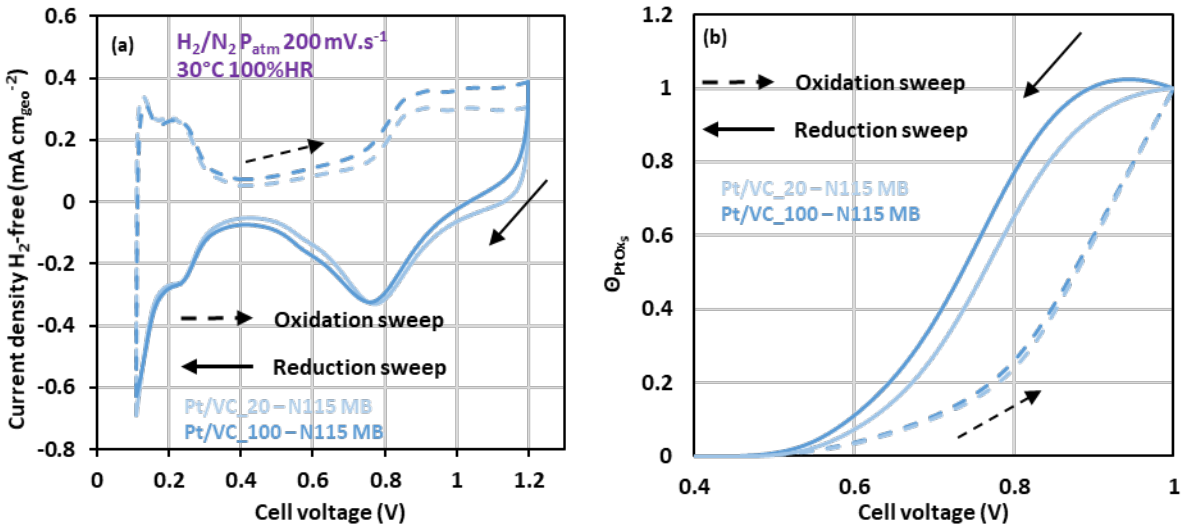


*Figure 7: (a) Voltamograms (third cycle) normalized by the Pt active surface from proton desorption coulometry obtained at both 20 and 100 µg $cm_{Pt}^{-2}$ loadings at 30 °C 100% RH and (b) comparison of the evolution of Pt surface oxides coverage with potential.*

## 4. Conclusions

In this work, electrochemical characterizations are performed on low-loaded catalyst layers thanks to a differential cell setup of PEMFC, to better understand the electrocatalyst operation and its utilization in catalyst layer under various operating conditions, at two loadings: 20 and 100 $\mu g_{Pt}\ cm_{geo}^{-2}$. The lack of accurate description of what is at stake during catalyst layer transient operation in modeling motivates the characterization of thin "0D" catalyst layer (Pt/VC_20); at the small corresponding catalyst layer thickness, one hopes to get rid of mass-transport issues inside the CL, which allows to neglect transport phenomena and resulting heterogeneities through the thickness and helps developing a model involving the ORR mechanism described by direct kinetic equation and including the Pt surface state evolution. The choice of the different components as well as specific electrochemical measurement procedures were also investigated and justified to characterize the Pt/VC_20 catalyst layers in the most reliable and relevant way. These electrochemical characterizations on Pt/VC_20 catalyst layers provide a reliable dataset using well-defined and well-known compositions so that the modeling description can be improved. Then, catalyst layers loaded at 100 $\mu g_{Pt}\ cm_{geo}^{-2}$ (Pt/VC_100) are also characterized for the same purposes, while adding mass- and ionic-transport losses of the catalyst layer (the so-called 1D configuration with a non-negligible catalyst layer thickness).

Electrochemical performance along the polarization curve under oxygenated atmosphere and the ohmic resistance evolution during the cathode catalyst layer operation are investigated under various operating conditions of temperature and hygrometry (relative humidity). Increasing the temperature and relative humidity leads to higher performance and promotes the Pt oxidation/reduction, which is ascribed to the enhanced kinetics of ORR (reduction of activation losses) and improved ionic mobility when increasing temperature with fully hydrated inlet gases. To get more insights, the hydration state of the membrane, estimated via the ohmic resistance evolution under the various operating conditions considered in this study, was also evaluated. When using fully hydrated inlet gases, the high frequency resistance is almost only increasing when lowering the potential (increasing the current density). On the contrary, using partially-hydrated inlet gases (at 50 and 80% RH) induces a first hydration of the membrane ($R_{HF}$ is decreasing), due to water production when the current density is increased, and then a dehydration of the membrane ($R_{HF}$ is increasing), due to local heat production (an antagonist phenomenon) when increasing more the current density. Additionally, the evolution of the hydration state of the membrane (estimated via the ohmic resistance evolution), allows to accurately correct the polarization curve from the ohmic drop. The performance hysteresis is still observed after this correction, which indicates that another contribution must be considered to explain the different performance during transient operation between the forward and backward sweeps of the polarization curve. As the very thin Pt/VC_20 catalyst layers are considered as

"0D", the remaining contribution should be related to Pt and its surface state linked to Pt-oxides formation and reduction. The behavior of Pt under nitrogen atmosphere through potential cycling was characterized, especially in the Pt-oxides region (between 0.4 and 1 V), where Pt-oxides coverage is qualitatively investigated.

The increase of the loading seems not to change the global trends observed regarding the impact of temperature and relative humidity on the catalyst layer behaviour under various operating conditions. Nonetheless, increasing the loading adds another dimension, the thickness and results in a different operation of the catalyst layer through its thickness, which is closely linked to the transport properties of realistic catalyst layers. In fact, the "1D" catalyst layer operation becomes much more complex, as a lot of physico-chemical and electrochemical phenomena, including their interplay, make the understanding of its operation difficult with such experimental characterizations. However, some assumptions can still be made: i) saturation in the pores of the active layer changes the accessibility of Pt to protons, and ii) the Pt surface state is potential dependant and is impacted by the Pt-oxides formation and reduction, but also by the ionomer adsorption/desorption onto Pt sites. To go further and to evaluate some hypothesis, advanced experimental characterization, generally time consuming and expensive, are mandatory. Thus, it is useful to analyse the raw experimental data with as comprehensive as possible physical models, which often implies numerical simulation. This will be the objective of the second part of the study "Low-Loaded Catalyst Layers For Proton Exchange Membrane Fuel Cell Dynamic Operation Part 2: Modelling Study".

## Acknowledgments

The authors would like to warmly thank Dr. Florian Chabot for the helpful discussions about the study and Laure Guétaz for her expertise in SEM imaging. The authors (and in particular MC) are all expressing their gratitude to Prof. Elena R. Savinova, who has always been an immense source of inspiration in their work. MC thank the "France 2030" government investment plan managed by the French National Research Agency (PEMFC95 project, grant ANR-22-PEHY-0005) for funding the post-doctorate of CL.

## References

[1] "FURTHER-FC project - Objectives." [Online]. Available: https://further-fc.eu/ABOUT-FURTHER-FC/OBJECTIVES/

[2] "CAMELOT - Overview." [Online]. Available: https://www.camelot-fuelcell.eu/index.php/about-camelot/overview

[3] M. Tempelaere, M. Zimmermann, and M. Chatenet, "3D-structured electrocatalysts for improved mass-transfer in proton-exchange membrane fuel cell cathodes," *Curr. Opin. Electrochem.*, vol. 41, p. 101353, Oct. 2023, doi: 10.1016/j.coelec.2023.101353.

[4] F. Chabot, J. Lee, F. Vandenberghe, L. Guétaz, G. Gebel, S. Lyonnard, L. Porcar, S. Rosini, and A. Morin, "Detailed Catalyst Layer Structure of Proton Exchange Membrane Fuel Cells from Contrast Variation Small-Angle Neutron Scattering," *ACS Appl. Energy Mater.*, vol. 6, no. 3, pp. 1185–1196, Feb. 2023, doi: 10.1021/acsaem.2c02384.

[5] M. Barreiros Salvado, P. Schott, L. Guétaz, M. Gerard, and Y. Bultel, "Optimization of Transports in a Proton-Exchange Membrane Fuel Cell Cathode Catalyst Layer at High Current Densities: A Coupled Modeling/Imaging Approach," *J. Electrochem. Soc.*, vol. 168, Art. no. 8, p. 084507, Aug. 2021, doi: 10.1149/1945-7111/ac1a84.

[6] M. Chatenet, L. Dubau, N. Job, and F. Maillard, "The (electro)catalyst|membrane interface in the Proton Exchange Membrane Fuel Cell: Similarities and differences with non-electrochemical Catalytic Membrane Reactors," *Catal. Today*, vol. 156, no. 3–4, pp. 76–86, Oct. 2010, doi: 10.1016/j.cattod.2010.02.028.

[7] R. Sgarbi, W. Ait Idir, Q. Labarde, M. Mermoux, P. Wu, J. Mainka, J. Dillet, C. Marty, F. Micoud, O. Lottin and M. Chatenet, "Does the platinum-loading in proton-exchange membrane fuel cell cathodes influence the durability of the membrane-electrode assembly?" *Ind. Chem. Mater.*, vol. 1, no. 4, pp. 501–515, 2023, doi: 10.1039/D3IM00059A.

[8] L. Dubau, L. Castanheira, F. Maillard, M. Chatenet, O. Lottin, G. Maranzana, J. Dillet, A. Lamibrac, J.-C. Perrin, E. Moukheiber, A. El Kaddouri, G. De Moor, C. Bas, L. Flandin and N. Caqué, "A review of PEM fuel cell durability: materials degradation, local heterogeneities of aging and possible mitigation strategies: A review of PEM fuel cell durability," *Wiley Interdiscip. Rev. Energy Environ.*, vol. 3, no. 6, pp.540-560, Nov. 2014, doi: 10.1002/wene.113.

[9] L. Dubau, L. Castanheira, M. Chatenet, F. Maillard, J. Dillet, G. Maranzana, S. Abbou, O. Lottin, G. De Moor, A. El Kaddouri, C. Bas, L. Flandin, E. Rossinot, and N. Caque, "Carbon corrosion induced by membrane failure: The weak link of PEMFC long-term performance," *Int. J. Hydrog. Energy*, vol. 39, no. 36, pp. 21902-21914, Dec. 2014, doi: 10.1016/j.ijhydene.2014.07.099.

[10] J. Wu, X. Zi Yuan, J. J. Martin, H. Wang, J. Zhang, J. Shen, S. Wu and W. Merida, "A review of PEM fuel cell durability: Degradation mechanisms and mitigation strategies," *J. Power Sources*, vol. 184, no. 1, pp. 104-119, Sep. 2008, doi: 10.1016/j.jpowsour.2008.06.006.

[11] C. Zhang, Z. Liu, W. Zhou, S. H. Chan, and Y. Wang, "Dynamic performance of a high-temperature PEM fuel cell – An experimental study," *Energy*, vol. 90, pp. 1949–1955, Oct. 2015, doi: 10.1016/j.energy.2015.07.026.

[12] M. Zago, A. Baricci, A. Bisello, T. Jahnke, H. Yu, R. Maric, P. Zelenay and A. Casalegno, "Experimental analysis of recoverable performance loss induced by platinum oxide formation at the polymer electrolyte membrane fuel cell cathode," *J. Power Sources*, vol. 455, p. 227990, Apr. 2020, doi: 10.1016/j.jpowsour.2020.227990.

[13] G. Soubeyran, F. Micoud, B. Morin, M. Reytier, and J. Poirot-Crouvezier, "Improved operating strategies for the optimization of PEMFC system performance," *J. Power Sources*, vol. 597, p. 234089, Mar. 2024, doi: 10.1016/j.jpowsour.2024.234089.

[14] T. Chu, Q. Wang, M. Xie, B. Wang, D. Yang, B. Li, P. Ming and C. Zhang, "Investigation of the reversible performance degradation mechanism of the PEMFC stack during long-term durability test," *Energy*, vol. 258, p. 124747, Nov. 2022, doi: 10.1016/j.energy.2022.124747.

[15] J. Mitzel, Q. Zhang, P. Gazdzicki, and K. A. Friedrich, "Review on mechanisms and recovery procedures for reversible performance losses in polymer electrolyte membrane fuel cells," *J. Power Sources*, vol. 488, p. 229375, Mar. 2021, doi: 10.1016/j.jpowsour.2020.229375.

[16] B. S. Pivovar and Y. S. Kim, "The Membrane–Electrode Interface in PEFCs I. A Method for Quantifying Membrane–Electrode Interfacial Resistance," *J. Electrochem. Soc.*, vol. 154, p. B739, May 2007, doi: 10.1149/1.2740005.

[17] N. Ge, R. Banerjee, D. Muirhead, J. Lee, H. Liu, P. Shrestha, A.K.C. Wong, J. Jankovic, M. Tam, D. Susac, J. Stumper and A. Bazylak, "Membrane dehydration with increasing current density at high inlet gas relative humidity in polymer electrolyte membrane fuel cells," *J. Power Sources*, vol. 422, pp. 163–174, May 2019, doi: 10.1016/j.jpowsour.2019.03.001.

[18] A. Damjanovic, M. A. Genshaw, and J. O. Bockris, "The Mechanism of Oxygen Reduction at Platinum in Alkaline Solutions with Special Reference to $H_2O_2$," *J. electrochem. Soc.*, vol. 114, no. 11, p. 1107, Mov. 1967, doi: 10.1149/1.2426425.

[19] A. Damjanovic and V. Brusic, "Electrode kinetics of oxygen reduction on oxide-free platinum electrodes," *Electrochimica Acta*, vol. 12, no. 6, pp. 615–628, Jun. 1967, doi: 10.1016/0013-4686(67)85030-8.

[20] A. Damjanovic, "New evidence supports the proposed mechanism for $O_2$ reduction at oxide free platinum electrodes," *Electrochimica Acta*, vol. 24, pp. 887–889, Nov. 1978, p. 3.

[21] H. Xu, R. Kunz, and J. M. Fenton, "Investigation of Platinum Oxidation in PEM Fuel Cells at Various Relative Humidities," *Electrochem. Solid-State Lett.*, vol. 10, no. 1, p. B1, 2007, doi: 10.1149/1.2372230.

[22] B. V. Tilak, B. E. Conway, and H. Angerstein-Kozlowska, "The real condition of oxidized pt electrodes: Part III. Kinetic theory of formation and reduction of surface oxides," *J. Electroanal. Chem. Interfacial Electrochem.*, vol. 48, no. 1, pp. 1–23, Nov. 1973, doi: 10.1016/S0022-0728(73)80290-6.

[23] D. E. Ramaker, A. Korovina, V. Croze, J. Melke, and C. Roth, "Following ORR intermediates adsorbed on a Pt cathode catalyst during break-in of a PEM fuel cell by in operando X-ray absorption spectroscopy," *Phys Chem Chem Phys*, vol. 16, no. 27, pp. 13645–13653, 2014, doi: 10.1039/C4CP00192C.

[24] E. L. Redmond, B. P. Setzler, F. M. Alamgir, and T. F. Fuller, "Elucidating the oxide growth mechanism on platinum at the cathode in PEM fuel cells," *Phys. Chem. Chem. Phys.*, vol. 16, no. 11, pp. 5301–5311, Feb. 2014, doi: 10.1039/C3CP54740J.

[25] M. Moore, A. Putz, and M. Secanell, "Investigation of the ORR Using the Double-Trap Intrinsic Kinetic Model," *J. Electrochem. Soc.*, vol. 160, no. 6, Art. no. 6, 2013, doi: 10.1149/2.123306jes.

[26] J. K. Nørskov, J. Rossmeisl, A. Logadottir, and L. Lindqvist, "Origin of the Overpotential for Oxygen Reduction at a Fuel-Cell Cathode," *J. Phys. Chem. B*, vol. 108, no. 46, p. 17886–17892, Nov. 2004, doi: 10.1021/jp047349j.

[27] H. S. Wroblowa, Yen-Chi-Pan, and G. Razumney, "Electroreduction of oxygen," *J. Electroanal. Chem. Interfacial Electrochem.*, vol. 69, no. 2, Art. no. 2, Apr. 1976, doi: 10.1016/S0022-0728(76)80250-1.

[28] A. A. McMath, J. van Drunen, J. Kim, and G. Jerkiewicz, "Identification and Analysis of Electrochemical Instrumentation Limitations through the Study of Platinum Surface Oxide Formation and Reduction," *Anal. Chem.*, vol. 88, no. 6, pp. 3136–3143, Mar. 2016, doi: 10.1021/acs.analchem.5b04239.

[29] H. Angerstein-Kozlowska, B. E. Conway, and W. B. A. Sharp, "The real condition of electrochemically oxidized platinum surfaces: Part I. Resolution of component processes," *J. Electroanal. Chem. Interfacial Electrochem.*, vol. 43, no. 1, pp. 9–36, Apr. 1973, doi: 10.1016/S0022-0728(73)80307-9.

[30] V. A. Saveleva, V. Papaefthimiou, M. K. Daletou, W. H. Doh, C. Ulhaq-Bouillet, M. Diebold, S. Zafeiratos, E. R. Savinova, "*Operando* Near Ambient Pressure XPS (NAP-XPS) Study of the Pt

Electrochemical Oxidation in $H_2O$ and $H_2O/O_2$ Ambients," *J. Phys. Chem. C*, vol. 120, no. 29, Art. no. 29, Jul. 2016, doi: 10.1021/acs.jpcc.5b12410.

[31] I. Martens, R. Chattot, M. Rasola, M. Valeria Blanco, V. Honkimäki, D. Bizzotto, D. P. Wilkinson, and J. Drnec, "Probing the Dynamics of Platinum Surface Oxides in Fuel Cell Catalyst Layers Using in Situ X-ray Diffraction," *ACS Appl. Energy Mater.*, vol. 2, no. 11, pp. 7772–7780, Nov. 2019, doi: 10.1021/acsaem.9b00982.

[32] B. E. Conway, "Electrochemical oxide film formation at noble metals as a surface-chemical process," *Prog. Surf. Sci.*, vol. 49, no. 4, pp. 331–452, Aug. 1995, doi: 10.1016/0079-6816(95)00040-6.

[33] G. Jerkiewicz, G. Vatankhah, J. Lessard, M. P. Soriaga, and Y.-S. Park, "Surface-oxide growth at platinum electrodes in aqueous H2SO4," *Electrochimica Acta*, vol. 49, no. 9–10, pp. 1451–1459, Apr. 2004, doi: 10.1016/j.electacta.2003.11.008.

[34] J. X. Wang, J. Zhang, and R. R. Adzic, "Double-Trap Kinetic Equation for the Oxygen Reduction Reaction on Pt(111) in Acidic Media," *J. Phys. Chem. A*, vol. 111, no. 49, pp. 12702–12710, Dec. 2007, doi: 10.1021/jp076104e.

[35] B. Jayasankar and K. Karan, "O2 electrochemistry on Pt: A unified multi-step model for oxygen reduction and oxide growth," *Electrochimica Acta*, vol. 273, pp. 367–378, May 2018, doi: 10.1016/j.electacta.2018.03.191.

[36] R. Ferreira de Morais, A. A. Franco, P. Sautet, and D. Loffreda, "Interplay between Reaction Mechanism and Hydroxyl Species for Water Formation on Pt(111)," *ACS Catal.*, vol. 5, no. 2, pp. 1068–1077, Feb. 2015, doi: 10.1021/cs5012525.

[37] T. Jahnke, G. A. Futter, A. Baricci, C. Rabissi, and A. Casalegno, "Physical Modeling of Catalyst Degradation in Low Temperature Fuel Cells: Platinum Oxidation, Dissolution, Particle Growth and Platinum Band Formation," *J. Electrochem. Soc.*, vol. 167, no. 1, p. 013523, Nov. 2019, doi: 10.1149/2.0232001JES.

[38] G. Maranzana, A. Lamibrac, J. Dillet, S. Abbou, S. Didierjean, and O. Lottin, "Startup (and Shutdown) Model for Polymer Electrolyte Membrane Fuel Cells," *J. Electrochem. Soc.*, vol. 162, no. 7, pp. F694–F706, 2015, doi: 10.1149/2.0451507jes.

[39] R. Riasse, C. Lafforgue, F. Vandenberghe, F. Micoud, A. Morin, M. Arenz, J. Durst and M. Chatenet, "Benchmarking proton exchange membrane fuel cell cathode catalyst at high current density: A comparison between the rotating disk electrode, the gas diffusion electrode and differential cell," *J. Power Sources*, vol. 556, p. 232491, Feb. 2023, doi: 10.1016/j.jpowsour.2022.232491.

[40] K. Broka and P. Ekdunge, "Oxygen and hydrogen permeation properties and water uptake of Nafion 117 membrane and recast film for PEM fuel cell.pdf," *J. Appl. Electrochem.*, vol. 27, pp. 117–123, 1997.

[41] M. Albaghdadi and H. Aljanabi, "Effect of operating parameters on the hygro–thermal stresses in proton exchange membranes of fuel cells," *Int. J. Hydrog. Energy*, vol. 32, no. 17, pp. 4510–4522, Dec. 2007, doi: 10.1016/j.ijhydene.2007.05.007.

[42] S. Ochi, O. Kamishima, J. Mizusaki, and J. Kawamura, "Investigation of proton diffusion in Nafion®117 membrane by electrical conductivity and NMR," *Solid State Ion.*, vol. 180, no. 6–8, pp. 580–584, May 2009, doi: 10.1016/j.ssi.2008.12.035.

[43] F. Nandjou, J.-P. Poirot-Crouvezier, M. Chandesris, S. Rosini, D.S. Hussey, D.L. Jacobson, J.M. LaManna, A. Morin and Y. Bultel, "A pseudo-3D model to investigate heat and water transport in large area PEM fuel cells – Part 2: Application on an automotive driving cycle," *Int. J. Hydrog. Energy*, vol. 41, no. 34, pp. 15573–15584, Sep. 2016, doi: 10.1016/j.ijhydene.2016.06.007.

[44] F. Vandenberghe, “Towards a better understanding and modeling of catalyst and catalyst layer operation in Proton Exchange Membrane Fuel Cell,” phdthesis, Université Grenoble Alpes [2020-....], 2022. Accessed: Jul. 03, 2024. [Online]. Available: https://theses.hal.science/tel-04137000

[45] L. Castanheira, L. Dubau, M. Mermoux, G. Berthomé, N. Caqué, E. Rossinot, M. Chatenet, and F. Maillard, “Carbon Corrosion in Proton-Exchange Membrane Fuel Cells: From Model Experiments to Real-Life Operation in Membrane Electrode Assemblies,” *ACS Catal.*, vol. 4, no. 7, pp. 2258–2267, Jul. 2014, doi: 10.1021/cs500449q.

[46] L. Castanheira, W. O. Silva, F. H. B. Lima, A. Crisci, L. Dubau, and F. Maillard, “Carbon Corrosion in Proton-Exchange Membrane Fuel Cells: Effect of the Carbon Structure, the Degradation Protocol, and the Gas Atmosphere,” *ACS Catal.*, vol. 5, no. 4, pp. 2184–2194, Apr. 2015, doi: 10.1021/cs501973j.

[47] L. M. Roen, C. H. Paik, and T. D. Jarvi, “Electrocatalytic Corrosion of Carbon Support in PEMFC Cathodes,” *Electrochem. Solid-State Lett.*, vol. 7, no. 1, p. A19, 2004, doi: 10.1149/1.1630412.